

Soft, hyper-elastic and highly-stable silicone-organo-clay dielectric elastomer for energy harvesting and actuation applications

Gregorio Boccalero^{a,b,}, Claire Jean-Mistral^c, Maila Castellano^b, Corrado Boragno^a*

^aDepartment of Physic, University of Genova, via Dodecaneso 33, 16146, Genova, Italy

^bDepartment of Chemistry and Industrial Chemistry, University of Genova, via Dodecaneso 31, 16146, Genova, Italy

^cLaboratoire de Mecanique des Contacts et des Structures, LaMCoS, University of Lyon, 18-20 rue de la science, 69621, Villeurbanne, France.

Abstract:

A new type of soft composite is archived by the use of two grade of commercially available Pt-catalyzed silicone elastomers and organic nanoclays (montmorillonite). A complete characterization underlines their attractive performances: lower Young modulus, higher dielectric permittivity, but without compromising important properties such as low dielectric losses and lower viscous losses, higher dielectric breakdown strength, and thereby maintaining the mechanical integrity of the elastomers. A figure of merit is introduced to compare all the innovative synthesized soft composites, characterized by a bimodal network. These achievements can be exploited for both the actuation and the energy generation purposes.

Keywords: A. Polymer-matrix composites (PMCs); A. Smart materials; B. Mechanical properties; B. Electrical properties.

* Corresponding author; Email: gre.boc@gmail.com.

1. Introduction

Deeply investigated in the last three decades as actuators, Dielectric Elastomers (DEs) can be also exploited as generators [1], representing a promising electromechanical transducer technology [2–5]. Dielectric Elastomer Generator (DEGs) consist in high permittivity elastomeric material, typically films or membranes, coupled with two stretchable electrodes. Silicone elastomers are one of the most used materials for DEGs, due to their high energy density, fast response and low viscous losses, compared to, for example, acrylics or polyurethanes [6,7]. Silicones are deeply adopted also in medical technology and in a broad range of industrial and manufacturing areas. The properties that make them a popular choice are water, UV, ozone and oxygen resistance, thermal stability over a wide range of temperatures, resiliency and flexibility even after curing, usability as solid or liquid and chemical resistance. Such properties are very attractive for the applications where safety and flexibility are primary requirements [8]. Silicone elastomers develops a quite low permittivity, typically between 2 and 3. Many studies have focused on increasing the dielectric permittivity through the use of high-permittivity metal oxide fillers (titanate oxide TiO_2 , barium titanate oxide BaTiO_3 and aluminium oxide Al_2O_3) leading to increasing the energy density of the material, and thereby decreasing the necessary driving voltages [9]. However, the stiffness of such composite-type systems increases significantly, thereby decreasing achievable strain and increasing the necessary driving voltage. [7] A solution could be increasing dielectric permittivity while decreasing Young's modulus in order to achieve a synergistic impact on lowering the driving voltage. This includes the use of solvent techniques [10], bimodal networks [11] and blends, such as poly-dimethyl-siloxane (PDMS)/poly-hexyl-thiophene (P3HT) [12], PDMS/polyethylene glycol (PEG) [13], and PDMS/cyano-propyl-functional PDMS matrix [14], where the cyano-functional PDMS acted both as a high permittivity filler and plasticiser. These systems showed improved electromechanical strain response, since both increased dielectric permittivities and decreased Young's modules were obtained. On the other side, decreasing the

Young's modulus typically increases the viscous losses, hysteresis and tear strength, and decreases the long-term stability and lifetime of the material. For DEGs applications, the ideal material must have a high dielectric permittivity, high electric breakdown field, low Young modulus, low electric and mechanical losses, high stability and lifetime. The reader is referred to Madsen et al.[9], Brochu et al.[6] and Koh et al.[5] for a complete and comprehensive description on dielectric elastomer design optimization. Other studies explored the effect of adding nanoclay to the silicone matrix, founding interesting results in terms of final permittivity, thermal conductivity and electrical breakdown voltages of the composites, despite a big compromise in terms of mechanical properties, such as the already cited increasing of modulus and related losses [15–17]. In this work, a new approach for the realization of soft silicone elastomer composites through the use of organic-modified nanoclays is presented. Our DEs develop increased dielectric permittivity and elastic strength, but without compromising important properties such as dielectric and viscous losses, and dielectric breakdown strength.

2. Materials and Methods

Two grades of silicone were selected as elastomeric matrix: a RTV silicone elastomer (Sylgard186 from Dow Corning) and a LSR silicone (Silbione 4310 PEX from Bluestar Silicones). Both materials are bicomponents, contain fumed silica, are cross-linked by a hydrosilylation reactions catalysed by highly active platinum catalysts (Karstedt's catalyst), and show medium-high viscosity when mixed (around 10^5 cP). Cloisite®20A from BKY, named OMMT in the rest of this paper, is an organo-modified nanoclay (montmorillonite) with a dimethyl, dehydrogenated tallow, quaternary ammonium salt surface-modifier (95 meq/100g of clay), in order to improve the compatibility with the silicone chains.

For both silicone matrix, the nanoclay was added in the component which not contain the catalyst (through a three roll to roll mill, model EXACT 80E), to avoid its partial inhibition. A Speed Mixer (Hauschild 2750) is used to mix this filled part with the second part

of the silicone. The samples compositions are reported in Table 1. Thin films, of 150 μm of thickness, were realised using an automatic bar coater armed with a 16 μm spiral wire cylinder, with a moving speed of 50 mm/min. To remove the gas bubbles inside the material, a vacuum chamber, applying 0.7 bar during 20 minutes, was used. Moreover, as reported in Table 1, Sylgard 186 was also prepared in presence of Dicumyl Peroxide (1 wt%). Films of 300 μm were obtained by using, a thin copper mask, and an hot hydraulic press at 70 bar, 180°C for 40 minutes.

Tensile tests were performed by a Lloyd 1KN tensile machine equipped by a 10N (+/- 0.1 mN) force sensor interfaced to a computer. The dog bone specimens (NF T 51-034 Standard, derived from Iso 527-1/37-2, Type H3) with thickness between 150 and 300 μm , were used. The measurements were carried out at 25°C with an elongation rate of 20 mm/min. Cyclic stresses at 200% of elongation, strength at break, elongation at break and percentage in stress losses between loading and unloading of the samples ($\sigma_{\%loss}$) were evaluated. Young modulus was estimated by fitting the experimental results of 5 specimens per sample with the Yeoh polynomial equation:

$$\sigma_m = \left(\lambda - \frac{1}{\lambda^2} \right) (2C_1 + 4C_2(I_1 - 3) + 6C_3(I_1 - 3)^2) \quad (1)$$

where σ_m is the mechanical stress defined as the ratio between measured force and the initial cross-sectional area of the specimen, λ is the stretch ratio (final length/initial length), $I_1 = \lambda^2 + 2\lambda^{-1}$ is the first invariant of the strain tensor for uniaxial deformation. C_1 , C_2 and C_3 are the material mechanical parameter, and $2C_1 = G$ represents the shear modulus. For silicone elastomers, the Poisson coefficient ν is between 0.485 and 0.495 therefore the equivalent Young modulus corresponds to about 3 times the shear modulus ($E = 2(1 + \nu)G \approx 3G$).

Dynamic Mechanical Analysis was performed through an Alton Paar Rheometer (Rheocompass) on rectangular thin samples with length of 40 mm and width of 10 mm. Firstly, an amplitude sweep test (AS) at 0.1 Hz in a range of 0.001-0.2 % of strain was performed in order to evaluate the linear viscoelastic region (LVE), at 25°C. Then, frequency sweep tests

(FS) at a fixed amplitude (inside the LVE) in a frequency range of 0.01-1 Hz were evaluated at different temperatures (from -20 to 80 °C) using a Solid Rectangular Fixtures (SRF) system.

Dielectric spectroscopy (DS) was performed with a Novocontrol BDS 20 GmbH dielectric analyser. The DE samples were sandwiched between two 50 nm Au/Pd (80:20) electrodes obtained through a metal evaporator (Quorum Q150 T ES). Then, each sample was placed on a conductor substrate (deposited gold wafer) inside an hermetic measuring chamber. Two gold needles, one on the top electrodes and one on the bottom conductor substrate insured the contacts. Permittivity (ϵ_r) and dielectric losses ($\tan\delta$) were evaluated using 3 V AC Voltage in the range of 10^{-1} - 10^6 Hz at 25°C on three samples for each material.

Electrical breakdown tests were performed in an in-house-built device based on international standards (IEC 60243-1 (1998) and IEC 60243-2 (2001)). The samples, prepared with same procedure adopted for the dielectric spectroscopy, were placed between two cylindrical electrodes (radius of 8 mm). A stepwise increasing voltage of 100 V from 0 to 12 KV in 200 s was applied and breakdown voltage was recorded. Thanks to the test conditions, the sample thickness is assumed to remain constant; a digital calliper checked this point. The breakdown strength of each sample was given by the average of 3 measurements.

Thermo-gravimetric analysis (TGA) was performed by a TGA/DSC 1 STAR^e System from Mettler Toledo in a nitrogen atmosphere with a heating rate of 10 °C/min from 25 to 900 °C to evaluate the filler amount in the materials.

Swelling measurements were conducted in cyclohexane. A thin layer sample of about 0.3 g (150-300 μm), was weighted for evaluating the initial dry weight (W_i) and plunged in 100 ml of cyclohexane in a Petri dish. The weight was evaluated during 3 days seeking its equilibrium value (plateau). Then, the sample was extracted, gently wiped to remove the liquid solvent present on the sample surface and immediately weighted (W_s). The sample was then dried overnight at 70 °C under vacuum and reweighted (W_f).

The volume fraction of the swollen sample was calculated as:

$$V = \frac{W_i - W_f c}{W_f - W_i c + (W_s - W_f) \frac{\rho_p}{\rho_s}} \quad (2)$$

where c represents the filler weight fraction, ρ_s and ρ_p the density of the solvent and polymer respectively. From this volume fraction, it is possible to estimate the average molar mass between cross-links, M_c , via the Flory–Rehner equation [18]:

$$M_c = \frac{-M_s \frac{\rho_p}{\rho_s} (V^{\frac{1}{3}} - \frac{V}{2})}{\ln(1 - V) + V + \chi V^2} \quad (3)$$

with M_s the molar mass of solvent, and χ the Flory-Huggins interaction parameter, which in case of PDMS-cyclohexane equals 0.44 [19]. The cross-link density ν was calculated as $\nu = \rho_p/M_c$.

The morphology of the materials was investigated using an integrated compact Transmission Electron Microscope (TEM) Jeol JEM 1011, operating at 100 KV, equipped with a Gatan Orius SC-1000 CCD camera. Ultra-thin samples, required for TEM analysis, were prepared by the use of a cryo-system and a specific diamond. Slices were collected and laid down onto a 200 mesh Vinylec/carbon-coated copper TEM grids, and then analyzed.

In order to evaluate the performance of a DEs realized, a method derived from Sommer-Larsen and Larsen[10] was developed: the latter was based on the calculation of the figure of merit, F_{om-SL} , originally defined as $F_{om-SL} = 3 \varepsilon_0 \varepsilon_r E_B^2 / E$ with ε_0 the vacuum permittivity, ε_r the permittivity, E_B the electrical breakdown and E the Young modulus of the DE. The figure of merit proposed in this work is instead defined as $F_{om} = 3 \varepsilon_0 \varepsilon_r \tan(\delta) E_B^2 G'' / E$, where $\tan(\delta)$ and G'' were introduced for taking into account also the related losses. F_{om} was used for the estimation of the final performances of our silicone composites.

3. Results and Discussions

3.1 Effect of OMMT on Pt-catalyst cross-link

As reported in literature, the quaternary ammonium salt used as surface modifier in the OMMT poisons the Pt-catalyst, rendering the latter inactive [20,21]. Therefore, a decrease of the cross-link degree with the increase of the amount of OMMT should be obtained. In fact, only the composites with an amount of filler which not exceeded 4 wt% of OMMT properly cross-linked. In order to obtaining Sylgard186-based composites with higher loading of OMMT (4 and 10 wt%), dicumyl peroxide (1 wt%) was adopted for forcing the cross-link. In Table 1, all the composites prepared are reported.

3.2 Mechanical characterization

All materials were well described by an hyper-elastic model (Eq.1), where the predominant term, linked to the elastic modulus E , was the first coefficient C_1 . As clearly shown in Fig. 1a, the pristine sample SY0 exhibited similar values of E as the one reported by the supplier and other studies in literature [6,9] ($E=0.9$ MPa). The LSR sample B0 are more flexible with an elastic modulus of 0.52 MPa and silicone with dicumyl peroxide SP0 embraces a higher value ($E=1.52$ MPa). Sylgard 186 cured with 1 wt% Dicumyl Peroxide showed the typical effect of adding fillers: the stiffness of the composites increases as the concentration of fillers increases ($E_{SP4MT}=1.65$ MPa and $E_{SP10MT}=2.05$ MPa). On the contrary, the filled RTV and LSR samples need less force to be stretched at the same ratio, leading to lower equivalent Young modulus for silicone composite: from 0.52 MPa to 0.17 MPa for LSR samples and from 0.87 MPa to 0.24 MPa for RTV silicone. These interesting and not usual results [9] pose the basis for a new and original approach for the design of DEs. **Fig. 1b** reports the cyclic deformation tests at 20 mm/min for the LSR samples, revealing that a steady state appears after 3 cycles for all tested materials underlying a very low Mullins effect even with fillers. Hysteresis and associated viscous losses remain low for pristine and composite materials. Surprisingly, the samples loaded with OMMT shown comparable losses with respect to the pristine material. Similar results have been obtained for the RTV samples, also showing reduced losses for the maximal loading. No plastic effects and no dependence with the strain rate occurred (tests were

also performed from 20 to 1000 mm/min), confirming, as reported in literature [9], the advantage of silicones. Furthermore, relaxation tests (not reported in this work) underline a global loss of stress measured for both materials (OMMT loaded RTV and LSR) lower than 5%. From a structural point of view, our systems showed bimodal network features, composed by a chemical network and a physical network. The chemical network, was formed by long and short chain fractions and low molecular mass molecules from the surface modifier of the fillers, where a part of the latter (quaternary ammonium salts) partially avoided its formation. On the other hand, a secondary network composed by the filler loading (fumed silica and nanoclay) consisted in a physical network which provided stability to the primary one. The result of such bimodal network was an improvement of all mechanical properties (less losses), despite the elastic modulus was reduced. Similar observations (low viscous losses with lower modulus) have been made by Madsen et al. [11] and Bejenarius et al.[22] in their studies focused on heterogeneous bimodal networks. This abnormal behaviour was attributed to a specific network formation rather than network artefacts. Shah et al. also observed reduced mechanical losses in silicone hybrid bimodal networks through the use of functionalized titania providing bridging chains and creation of localized short spaced cross-links [23].

3.3 Rheological characterization

As it can be noted in **Fig. 2a** and **Fig. 2b**, the values of G' obtained overestimated the expected values (see **Fig. 1a**): for instance, B2MT and B4MT at 20°C show G' around 2 MPa for rheological characterization but only 0.24 and 0.17 MPa respectively, for the tensile test. Geometry of the sample (H3 and rectangular one) could explain this change. Indeed, the change of the geometry of thin samples affected the results of G' and G'' obtained by the DMA measurements. Dessi et al.[24] highlighted the effect of a non-linear stress distribution acting on soft samples in particular geometries due to the deformation imposed in the measurements, and proposed a correction. Nonetheless, the correction proposed by Dessi et al. provided an underestimation of the modulus (see **Fig. 2c**). For all these reasons, the rheological behaviour of the materials allows us only to point out the filler-matrix interaction through studies led at very

low deformation (0.001-0.2%). The abnormal behaviour of composite is also underlined: decrease of Young modulus as the amount of fillers increases. All material, except SY4MT and B4MT (the more loaded composites), showed temperature dependence on storage modulus G' and loss modulus G'' , similarly to the case reported in **Fig. 2a**. The case of B4MT is reported in **Fig. 2b**: similarly to SY4MT, G'' show the same answer at all temperature and all frequencies, especially at the highest ones. G'' behaviour is strictly linked to the rheology of particles, small molecules and dangling chains: increasing the temperature, they give more movement to the long chains, thus increasing the energy losses while decreasing the values of G' . In fact, at low frequencies the dangling chains and small molecules have enough time to react to the slow deformations (Reptation effect [25]), while at higher frequencies they should tend to flow (liquid-like behaviour). All the materials analyzed (SY0MT, SY2MT, SY4MT, B0, B2MT and B4MT) showed this behaviour in G' over 0.2 Hz. For SY4MT and B4MT, probably due the differences in filler level of dispersion and the presence of more physical cross-links, more stability both in temperature and frequency deformation was observed, suggesting the formation of an efficient bimodal network system.

3.4 Dielectric Spectroscopy

At low frequencies, dielectric spectroscopy showed an enhancement of performance in almost all samples loaded with OMMT respect the pristine ones: increase of the permittivity with small increase of the losses. However, the trends of both permittivity and dielectric losses possessed very different behaviour when clay is added. For Sylgard 186 with dicumyl peroxide composites, a classical behaviour is notified as reported in literature: linear increase in permittivity and losses with the amount of fillers, and exponential increase in permittivity with decreasing frequency [17]. Conversely, a non-monotonic behaviour is highlighted with RTV and LSR samples. For RTV samples, a bell-shape on the permittivity values as a function of the amount of fillers is underlined: for SY0MT $\epsilon_r@40 \text{ Hz} = 2.81$ (close to the supplier value) for SY2MT $\epsilon_r@40 \text{ Hz} = 3.38$ (+26%) and for SY4MT $\epsilon_r@40 \text{ Hz} = 3.10$ (+11%). Similar non-linearity

were also observed for LSR samples when filled: for BO $\epsilon_{r@40 \text{ Hz}} = 2.73$, for B2MT $\epsilon_{r@40 \text{ Hz}} = 2.7$ (quite same value as pristine sample), while for B4MT $\epsilon_{r@40 \text{ Hz}} = 3.1$ (+18%). These non-monotonic trends could be explained through the different levels of the clay dispersion, able to forming mono or poly-disperse fractal aggregates if a proper flocculation is not guaranteed[26], thus causing different dielectric contributes. The effect of organically modified montmorillonite (OMMT) on the dielectric properties of silicone rubber was examined by Razzaghi et al.[17] in two concentration levels similar to the ones used in this study, 2 and 5 wt%. They underlined that the order of organo-clay layers in the less dispersed structure imparts an additional ionic polarization and higher dielectric permittivity compared to clay layers that are more dispersed and have lost their order. Finally, in **Fig. 3b** the losses for RTV composites samples, showed an increase with the amount of fillers, basically due to interfacial polarization phenomena between electrode and polymer, and/or between polymer and filler such as accumulation of space-charges at the interfaces/interphases of the materials [27]. Differently to the analysis of permittivity, the losses appeared coherent with the amount of filler, and smaller respect what found in literature [16], reaching values of less than 0.03 in the cases of highest filling. For the reasons stated, the composites seemed belonging to particular dispersion conditions of the clay. Deeper investigations, out of the scope of this paper, could confirm our assumptions.

3.5 Electrical Breakdown measurements

The breakdown electric field evaluated by the electrical breakdown measurements revealed that the adding of OMMT imparts benefits to the system also from this point of view. The results are reported in Table 4. All samples containing OMMT showed higher breakdown strength E_B with respect to pristine materials, excepted for SY2MT, for which the values was comparable with SY0. E_B for B4MT appeared higher than B0 but slightly lower than B2MT. We interpreted this results with the order of dispersion of the nanoclays, as the previous analysis suggested, and similarly to whom reported from Yi et al. [27]. Moreover, it is well known that a decrease in the Young's modulus due to the reduce of the cross-link density normally produces a less

electromechanical stability. Conversely, a contemporary reduction of chemical cross-links of the matrix, increase of physical cross-links due to clay, and possible presence of reinforcing filler macro-island, gives the possibility of an enhancement of electro-mechanical integrity. Consequently, these are further beneficial and not usual effects.

3.6 Thermo-gravimetric analysis

By taking into account the previous results, TGA were performed exclusively on LSR samples (B0, B2MT, B4MT), the more promising for our goals. **Fig. 4** reports the degradation curves under nitrogen atmosphere of B0, B2MT, B4MT and of each part of formulation of B0. The two parts, named B0_A and B0_B, are prepared from the same base, i.e., silica and a vinyl-terminated PDMS. B0_A additionally contains the platinum catalyst, whereas B0_B adds on a few percent of hydrido-functionalized silicone chains as a cross-linker [28]. The latter degraded at lower T with respect B0, and same effect was observed for B2MT and B4MT, coherently with the decrease of cross-link expected. All formulations behaved similarly, with no significant degradation taking place before 250°C, and a slow degradation up to around 500°C, where weight losses of about 10% were detected. B2MT and B4MT showed a degradation between 300 and 350°C, which was not shown in B0. An increase of percentage residue at 900 °C by increasing the OMMT content was observed; on the other hand, the values obtained seemed higher with respect the filler contents estimated. Delebecq et al.[28] carried out an exhaustive TGA study on silica-PDMS model samples, mimicking high-temperature vulcanizing (HTV) silicone and LSR formulations. They found out that without platinum in the recipe all the PDMS chains de-polymerized into volatile cyclosiloxanes, leading to no residue. With platinum, the residue content depended on the silica content and silica surface modification because an induced ceramization occurred. B0_B showed a 19.6% of residue, thus attributed to the silica content, while B0_A revealed a 26.9% of residue, 7% more than B0_B. The final residue measured for B0 was higher than B0_A, indicating a further ceramization occurred in presence of highly constrained cross-linked chains around silica [27]. Similarly, when OMMT was added to the system an induced ceramization residue was observed: the difference in residues was

coherent with the OMMT amount (see Table 2). The OMMT ceramization is a sought-after fire protection property deeply exploited in industry [29].

3.7 Swelling measurements

The LSR-based samples showed a maximum in percentage of swelling very high, as it can be noted in Table 3, corresponding to the maximal distension of the silicone chains in the presence of a good solvent as cyclohexane. By the use of the filler weight fraction obtained from TGA, the cross-link density and the extracted material (related to the gel fraction) of the LSR samples were calculated. By increasing the amount of OMMT, the cross-link degree density decreased, while the averaged molar mass between cross-links, M_c , increased, as expected because of the partial inhibition of the cross-link catalyst. The evaluated M_c appeared moderate if compared to the values reported literature [30], meanwhile the extracted material was less than 2%. The latter also slightly increase with the amount of OMMT. Swelling measurements confirmed the observation from the previous analysis.

3.8 TEM analysis

Despite the difficulty of preparation of the samples through the microtomy process, mainly because of their very low thickness and high softness, a representative TEM image of the representative composite B2MT is reported in **Fig. 5**. It can be noted that the clays are partially packed in macro regions, surrounded by the silicone matrix and silica particles (well displayed because of the transmission beam), and partially dispersed in single palettes (highlighted with circles).

4. Conclusions

New soft dielectric elastomers matrix with improved performances were prepared through the use of commercially available RTV silicone rubber, LSR and organo-modified nanoclay. The competition between a partial inhibition of the cross-linking, caused by the nanoclay surface modifier, and an increase of physical cross-links imparted by nanoclays and related filler stiffness, brought a decreases in Young's modules, without decreasing mechanical stability, and

thereby the lifetime of the dielectric elastomers. Conversely, a specific bimodal network, formed by silica nanoparticles, long siloxane chains and aggregations of exfoliated nanoclays, decreases the viscoelasticity of the materials. An increase of dielectric permittivities were obtained for all films containing OMMT, while dielectric losses remained at a very low level. Electrical breakdown strength also improved with OMMT respect to pristine materials. The synergistic effect of reducing elastic modules, increasing dielectric permittivity and dielectric breakdown strengths thus resulted in globally improved performances. Despite the permittivity of the materials realized did not reach extraordinary values, the dielectric and mechanical losses remained very low, though by decreasing the Young modules. Indeed, we underline that the literature proposed very high performance composite materials, but characterized by too high stiffness or too high losses for our scopes [9]. Using the figure of merit proposed in this work, which considered also the mechanical and electrical losses, our materials appeared very promising (see Table 4). Such interesting performances could be exploited both for actuation and generation purposes [31–33].

Acknowledgements

G.B. thanks the partial support from the MIUR - PRIN 2012 project n. D38C13000610001, funded by the Italian Ministry of Education and SEASEA Project (DS0201) 2014, founded by the Agence Nationale Française de la Recherche. E. Lago and V. Pellegrini from IIT of Genova are thankful for the TEM images provided, and F. Ganachaud for his suggestions and for the interpretation of the results. We acknowledge A. Silvestre and C. Lagomarsini from G2ELAB of University of Grenoble-France for their collaboration regarding the dielectric measurements.

References

- [1] Boccalero G, Boragno C, Olivieri S, Mazzino A. FLuttering Energy Harvester for Autonomous Powering (FLEHAP): A synergy between EMc and Dielectric Elastomers

- Generators. *Procedia Eng.*, 2017. doi:10.1016/j.proeng.2017.09.489.
- [2] Perline R, Kornbluh R, Eckerle J, Jeuck P, Oh S, Pei Q, et al. Dielectric Elastomers: Generator Mode Fundamentals and Applications. *Electroact Polym Actuators Devices* 2001;4329:148–56. doi:10.1117/12.432640.
- [3] Jean-Mistral C, Basrour S, Chaillout J-J. Comparison of electroactive polymers for energy scavenging applications. *Smart Mater Struct* 2010;19:85012. doi:10.1088/0964-1726/19/8/085012.
- [4] McKay TG, O'Brien BM, Calius EP, Anderson IA. Soft generators using dielectric elastomers. *Appl Phys Lett* 2011;98:1–4. doi:10.1063/1.3572338.
- [5] Koh SJA, Keplinger C, Li T, Bauer S, Suo Z. Dielectric elastomer generators: How much energy can be converted? *IEEE/ASME Trans Mechatronics* 2011;16:33–41. doi:10.1109/TMECH.2010.2089635.
- [6] Brochu P, Pei Q. Advances in dielectric elastomers for actuators and artificial muscles. *Macromol Rapid Commun* 2010;31:10–36. doi:10.1002/marc.200900425.
- [7] Madsen FB, Yu L, Daugaard AE, Hvilsted S, Skov AL. A new soft dielectric silicone elastomer matrix with high mechanical integrity and low losses. *RSC Adv* 2015;5:10254–9. doi:10.1039/C4RA13511C.
- [8] Saleem A, Frommann L, Soever A. Fabrication of extrinsically conductive silicone rubbers with high elasticity and analysis of their mechanical and electrical characteristics. *Polymers (Basel)* 2010;2:200–10. doi:10.3390/polym2030200.
- [9] Madsen FB, Daugaard AE, Hvilsted S, Skov AL. The Current State of Silicone-Based Dielectric Elastomer Transducers. *Macromol Rapid Commun* 2016;37:378–413. doi:10.1002/marc.201500576.
- [10] Sommer-Larsen P, Larsen AL. Materials for dielectric elastomer actuators. *SMS*, vol. 5385, 2004, p. 5310–85.
- [11] Madsen FB, Daugaard AE, Fleury C, Hvilsted S, Skov AL. Visualisation and characterisation of heterogeneous bimodal PDMS networks. *RSC Adv* 2014;4:6939–45.

doi:10.1039/C3RA47522K.

- [12] Carpi BF, Gallone G, Galantini F, Rossi D De. Silicone-Poly (hexylthiophene) Blends as Elastomers with Enhanced Electromechanical Transduction Properties **. *Adv Funct Mater* 2008;18:235–41. doi:10.1002/adfm.200700757.
- [13] Liu H, Zhang L, Yang D, Ning N. A new kind of electro-active polymer composite composed of silicone elastomer and polyethylene glycol. *J Phys D Appl Phys* 2012;45:5303. doi:10.1088/0022-3727/45/48/485303.
- [14] Risse S, Kussmaul B, Krüger H, Kofod G. Synergistic Improvement of Actuation Properties with Compatibilized High Permittivity Filler. *Adv Funct Mater* 2012;22:3958–62. doi:10.1002/adfm.201200320.
- [15] Mishra S, Shimpi NG, Mali AD. Surface modification of montmorillonite (MMT) using column chromatography technique and its application in silicone rubber nanocomposites. *Macromol Res* 2012;20:44–50. doi:10.1007/s13233-012-0003-8.
- [16] Gharavi N, Razzaghi-Kashani M, Golshan-Ebrahimi N. Effect of organo-clay on the dielectric relaxation response of silicone rubber. *Smart Mater Struct* 2009;19:25002. doi:10.1088/0964-1726/19/2/025002.
- [17] Razzaghi-Kashani M, Gharavi N, Javadi S. The effect of organo-clay on the dielectric properties of silicone rubber. *Smart Mater Struct* 2008;17:65035. doi:10.1088/0964-1726/17/6/065035.
- [18] Flory PJ, Rehner J. Statistical Mechanics of Cross-Linked Polymer Networks II. Swelling. *J Chem Phys* 1943;11:521–6. doi:10.1063/1.1723792.
- [19] Dechant J. Polymer handbook. 3rd edition. J. BRANDRUP and E. H. IMMERGUT (editors). ISBN 0-471-81244-7. New York/Chichester/Brisbane/Toronto/Singapore: John Wiley & Sons 1989. Cloth bound, ca. 1850 pages, £ 115.00, \$175.00. *Acta Polym* 1990;41:361–2. doi:10.1002/actp.1990.010410614.
- [20] Lewis LN, Stein J, Gao Y, Colborn RE, Hutchins G. Platinum catalysts used in the silicone industry. *Platin Metals Rev* 1997;41:66–75.

- [21] Colas A. Silicones: Preparation, Properties and Performances. Dow Corning, Life Sci 2005:14.
- [22] Bejenariu AG, Yu L, Skov AL. Low moduli elastomers with low viscous dissipation. *Soft Matter* 2012;8:3917–23. doi:10.1039/C2SM25134E.
- [23] Shah J, Yuan Q, Misra RDK. Synthesis, structure and properties of a novel hybrid bimodal network elastomer with inorganic cross-links: The case of silicone-nanocrystalline titania. *Mater Sci Eng A* 2009;523:199–206. doi:10.1016/j.msea.2009.05.059.
- [24] Dessi C, Tsibidis GD, Vlassopoulos D, Corato M De, Trofa M, Avino GD, et al. Analysis of dynamic mechanical response in torsion Analysis of dynamic mechanical response in torsion. *J Rheol (N Y N Y)* 2016;60:275–87. doi:10.1122/1.4941603.
- [25] Giannelis EP, Krishnamoorti R, Manias E. Polymer-Silicate Nanocomposites : Model Systems for Confined Polymers and Polymer Brushes. *Adv Polym Sci* 1999;138:107–47.
- [26] Rueda MM, Auscher MC, Fulchiron R, Périé T, Martin G, Sonntag P, et al. Rheology and applications of highly filled polymers: A review of current understanding. *Prog Polym Sci* 2017;66:22–53. doi:10.1016/j.progpolymsci.2016.12.007.
- [27] Yi X, Duan HL, Chen Y, Wang J. Prediction of complex dielectric constants of polymer-clay nanocomposites. *Phys Lett A* 2007;372:68–71. doi:10.1016/j.physleta.2007.07.020.
- [28] Delebecq E, Hamdani-devareennes S, Raeke J, Cuesta L. High Residue Contents Indebted by Platinum and Silica Synergistic Action during the Pyrolysis of Silicone Formulations. *Appl Mater Interfaces* 2011;3:869–80. doi:10.1021/am101216y.
- [29] Anyszka R, Bielinski DM, Pedzich Z, Szumera M. Influence of surface-modified montmorillonites on properties of silicone rubber-based ceramizable composites. *J Therm Anal Calorim* 2015;119:111–21. doi:10.1007/s10973-014-4156-x.
- [30] Stricher a. M, Rinaldi RG, Barrès C, Ganachaud F, Chazeau L. How I met your elastomers: from network topology to mechanical behaviours of conventional silicone materials. *RSC Adv* 2015;5:53713–25. doi:10.1039/C5RA06965C.

- [31] Roy D. Kornbluh; Ron Pelrine; Qibing Pei; Richard Heydt; Scott Stanford; Seajin Oh; Joseph Eckerle. Electroelastomers: applications of dielectric elastomer transducers for actuation, generation, and smart structures. *Smart Struct. Mater., Proc. SPIE*, 4698; 2012, p. 254.
- [32] Kaltseis R, Keplinger C, Baumgartner R, Kaltenbrunner M, Li T, Mächler P, et al. Method for measuring energy generation and efficiency of dielectric elastomer generators. *Appl Phys Lett* 2011;99:10–3. doi:10.1063/1.3653239.
- [33] Carpi F, Anderson I, Bauer S, Frediani G, Gallone G, Gei M, et al. Standards for dielectric elastomer transducers. *Smart Mater Struct* 2015;24:25. doi:10.1088/0964-1726/24/10/105025.

Figure captions

Figure 1 - Mechanical parameters obtained by fitting the experimental curves (a) with the hyper-elastic Yeoh polynomial (eq. 1 with $R > 0.995$). Cyclic stress of the LSR-based materials from tensile tests at 20 mm/min (b), and an example of a normalized-stress-time curve in the top part.

Figure 2 - Frequency sweep (FS) at 0.01% strain of B2MT (a) and B4MT (b) varying T. In (c) FS at 20°C varying the amount of OMMT, applying the correction proposed by Dessi et al. [24].

Figure 3 - Dielectric Permittivity (a) and Losses (b) of the studied materials obtained by Dielectric Spectroscopy.

Figure 4 - Thermo-gravimetric Analysis (TGA) of Silbione samples: B0, B2MT and B4MT. Weight residue on the left ordinate axis and first derivative on the right ordinate axis.

Figure 5 - TEM images of B2MT: portion of aggregated and flocculated nanoclay plates. The circles highlight the flocculated condition of dispersion, reported in another image at lower magnification (barscale of 0.5 μm).

Table caption

Table 1 - Nomenclature of the material prepared.

Table 2 - Results obtained by TGA on LSRs (Silbione 4310-based samples).

Table 3 - Results obtained by swelling measurements of LSRs in cyclohexane.

Table 4 - Summary of the characterization of the materials realized. ¹TGA, ²Swelling (in cyclohexane), ³Tensile (Yeoh polynomial), ⁴Dielectric Spectroscopy (at 40 Hz), ⁵Electrical breakdown, Figure of merit, normalized to SY0 and B0, * proposed in Sommer-Larsen et al.¹⁰, and ** in this work.

Tables

Table 1 - Nomenclature of the material prepared.

Filler	Base material		
	Sylgard 186 (A+B) RTV	Silbione 4310 (A+B) LSR	Sylgard 186 (A+B+1 wt% peroxide)
0	SY0	B0	SP0
2	SY2MT	B2MT	-
4	SY2MT	B4MT	SP4MT
10	-	-	SP10MT

Table 2 - Results obtained by TGA on LSRs (Silbione 4310-based samples).

Formulation	OMMT wt%	T _{d2%} °C	T _{max} °C	Inorganic Residue wt%	Estimated silica wt%	Ceramiz. residue wt%
B0 _A (part A)	-	264	595	26.9	19.6	7.0
B0 _B (part B)	-	258	593	19.6	19.6	0
B0 (reticulated)	0	302	622	32.4	19.6	12.8
B2MT	2	297	601	36.5	19.6	14.9
B4MT	4	297	609	38.9	19.6	15.3

Table 3 - Results obtained by swelling measurements of LSRs in cyclohexane.

Material (Silbione 4310)	OMMT wt%	Max Swelling %	Equilibrium Swelling %	Extracted material %	M _c g/mol	ν mol/m ³
B0	0	481	462	1.66	6000	160
B2MT	2	458	418	1.82	8500	117
B4MT	4	452	365	1.99	11000	88

Table 4 - Summary of the characterization of the materials realized. ¹TGA, ²Swelling (in cyclohexane), ³Tensile (Yeoh polynomial), ⁴Dielectric Spectroscopy (at 40 Hz), ⁵Electrical breakdown, Figure of merit, normalized to SY0 and B0, * proposed in Sommer-Larsen et al.¹⁰, and ** in this work .

	SY0	SY2MT	SY4MT	B0	B2MT	B4MT
OMMT wt%	0	2	4	0	2	4
Silica wt% ¹	-	-	-	19.6	19.6	19.6
ν , in mol/m ³ ²	-	-	-	160	117	84
E , in MPa ³	0.87	0.48	0.24	0.52	0.35	0.17
$\sigma_{\%loss}$ ³	0.085	0.087	0.034	0.087	0.106	0.101
rupture % ³	280	170	220	690	1050	1151
ϵ' ⁴	2.73	3.54	3.14	2.75	2.75	3.23
$\tan(\delta)$ ⁴	0.0023	0.0118	0.0186	0.0038	0.0358	0.0404
E_B , in V/ μm ⁵	19.1	18.3	21.3	24.8	35.7	30.2
$F_{om-SL}/F_{om-SLSY0}$ [*]	1.0	2.2	5.3	2.8	8.9	14.9
$F_{om-SL}/F_{om-SLB0}$ [*]	-	-	-	1.0	3.1	5.3
F_{om}/F_{omSY0} ^{**}	1.0	11	105	5	110	225
F_{om}/F_{omB0} ^{**}	-	-	-	1.0	24	49

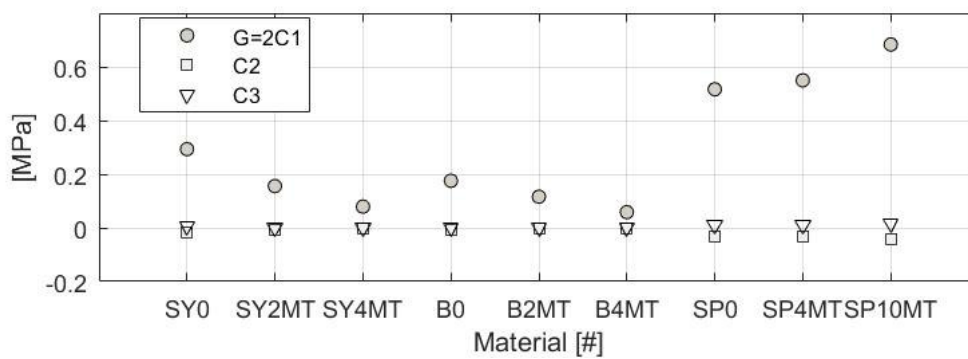


Fig. 1a

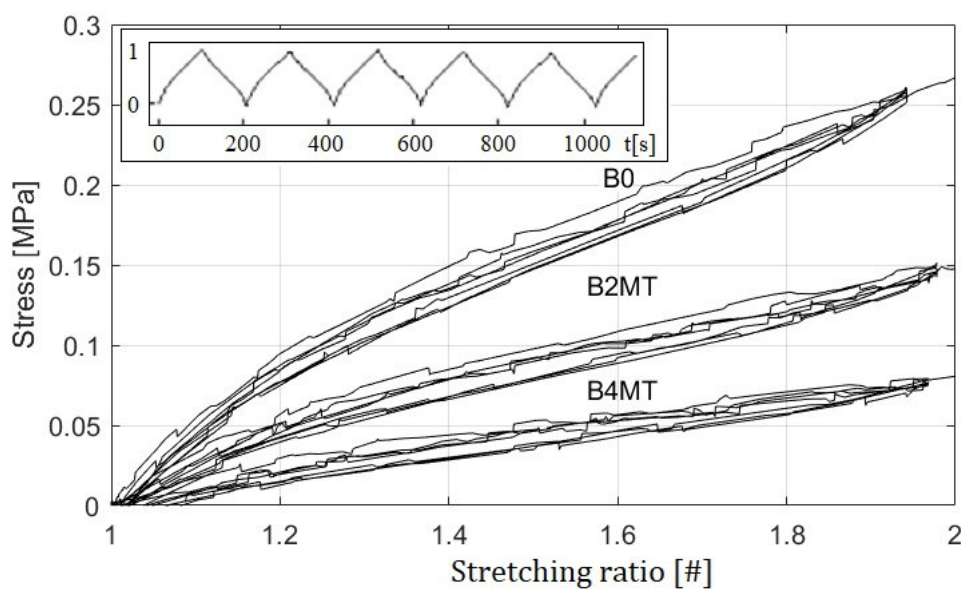


Fig. 1b

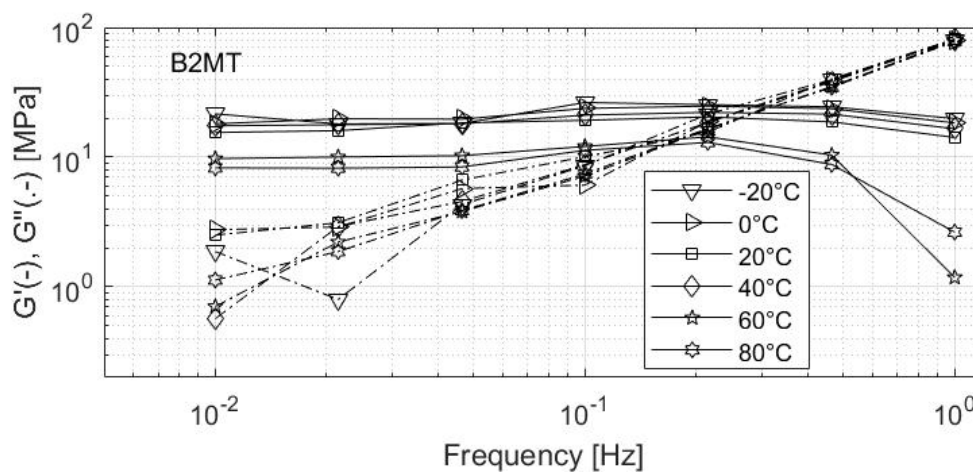


Fig. 2a

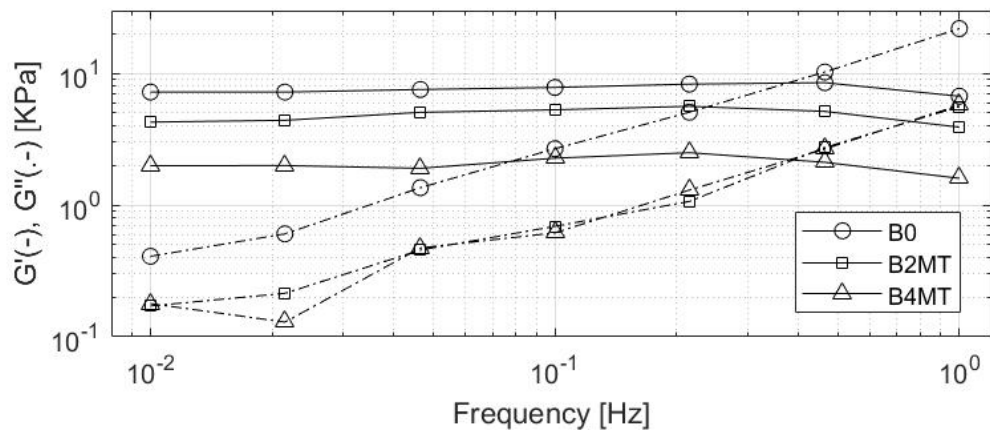


Fig. 2b

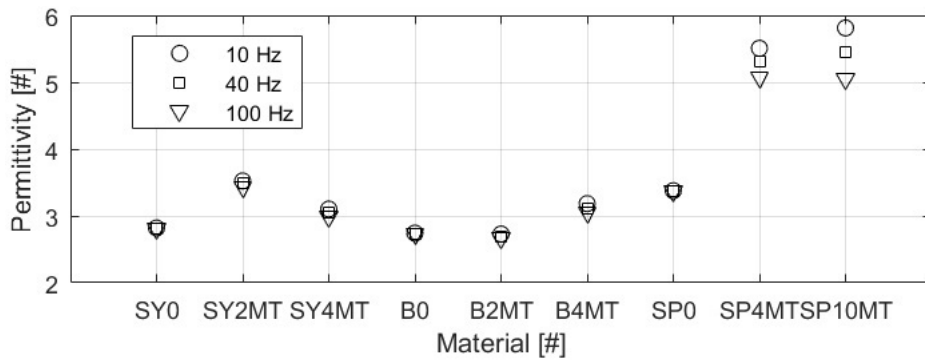


Fig. 2c

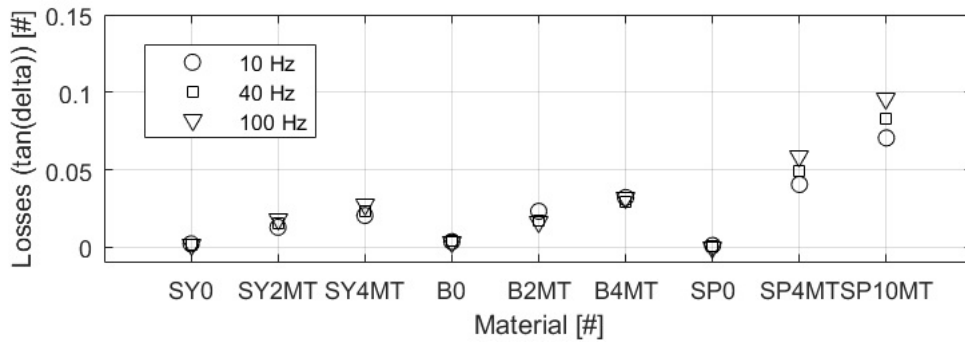


Fig. 3a

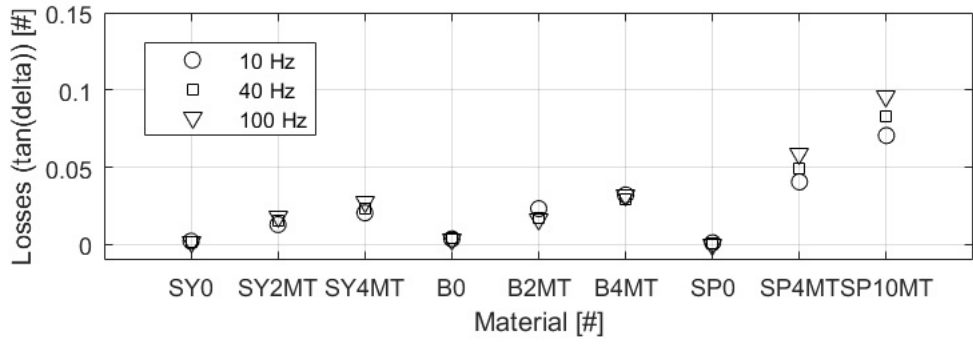


Fig. 3b

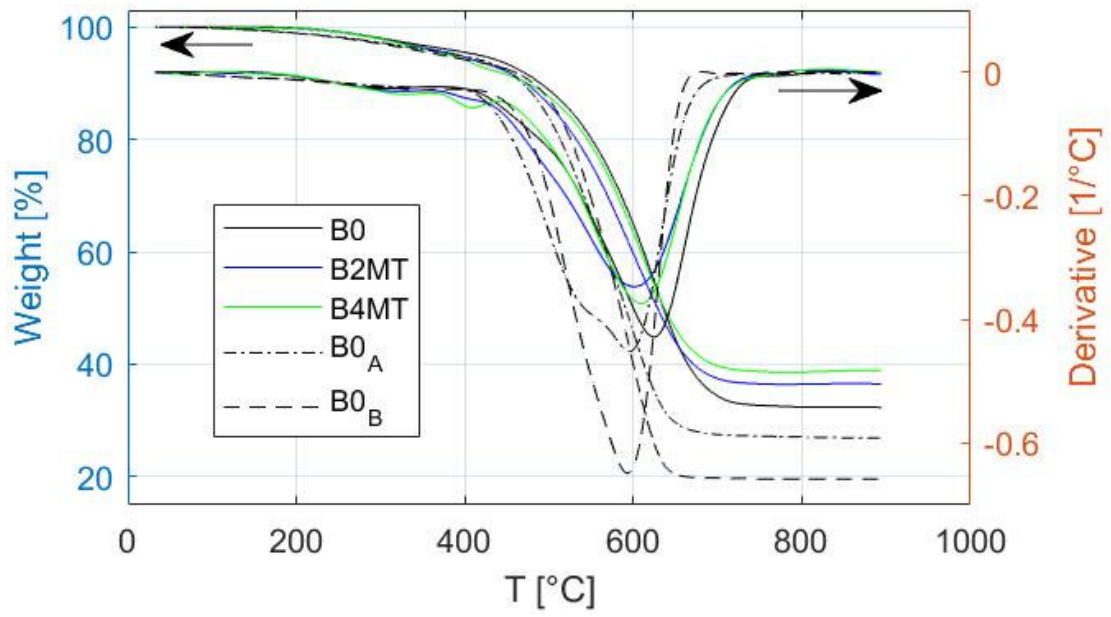


Fig. 4